Journal of Materials Chemistry A

COMMUNICATION

View Article Online
View Journal | View Issue

The synthesis of a core–shell MnO_2/3D-ordered hollow carbon sphere composite and its superior electrochemical capability for lithium ion batteries†

Cite this: *J. Mater. Chem. A*, 2014, **2**, 6343

Received 16th January 2014
Accepted 31st January 2014

DOI: 10.1039/c4ta00252k

www.rsc.org/MaterialsA

Zang Jun,‡ Chen Jia-jia,‡ Zhang Cheng-long, Qian Hang, Zheng Ming-sen* and Dong Quan-feng*

A hierarchical core–shell MnO_2/3D-ordered hollow carbon sphere composite was designed and synthesized by using hollow carbon spheres (HCS) as a carbon matrix. It exhibited excellent cycling stability and high current density performance with a stable and reversible capacity of 420 mA h g^{-1} at 1 A g^{-1} (based on the whole mass of the composite) and showed potential as a anode material for high power lithium ion batteries. The excellent performance of this MnO_2/HCS composite is due to the synergistic effect of the hierarchical architecture combined with nano-MnO_2 and the porous structure of HCS.

There are numerous ongoing research efforts focused on the search for carbon alternatives, in the hope of finding materials with both larger capacities and slightly more positive intercalation voltages compared to Li/Li^+, so as to minimize the risks of Li dendrite formation at the end of fast recharging, which is associated with safety problems. Such efforts have resulted in the emergence of transition metal oxides (TMOs) that could be considered as the most promising anode materials in next-generation lithium ion batteries (LIBs).[1,2] Among these TMOs, manganese oxides have attracted significant attention due to their various crystalline structures, which have different physical and electrochemical properties.[3–6] When used as an anode material the theoretical capacity of MnO_2 at a moderate discharge potential (~0.4–0.5 V *vs.* Li/Li^+) can be as high as 1233 mA h g^{-1} (based on a 'conversion mechanism'), which is among the highest known of TMOs and more than 3 times larger than that of a commercial graphite anode (372 mA h g^{-1}).[7–9] Meanwhile, it is a resource-abundant material and environmentally friendly.[10] In fact, birnessite-type MnO_2 with a high reversible capacity can be used as an anode electrode when the reversible conversion mechanism is enabled by the formation of nanometer-sized (<5 nm) Mn grains uniformly dispersed in a Li_2O matrix during the manganese oxide reduction reaction.[4,9] The nanometer-sized intact interface between the Mn grains and Li_2O makes the reverse reaction kinetically favorable. Nevertheless, the development of MnO_2 as an anode material for lithium ion batteries is still hindered by the inability to achieve a complete conversion reaction of MnO_2, volume changes and particle pulverization during the lithiation/delithiation process.[4,11]

It has been pointed out that decreasing the particle size to the nanoscale and combining with a conductive matrix, such as carbon nanotubes or graphene nanosheets, are effective ways to improve the electrochemical performance of TMO anodes.[12–14] The conductive matrix not only has the benefits of shortening the lithium ion transportation path ways and providing more convenient electron transfer, but accommodates volume expansion during battery cycling. Nevertheless, a previous investigation on MnO_2 as an anode material demonstrated only the partial conversion reaction of a MnO_2/carbon nanotube (CNT) composite, with a reversible capacity of 801 mA h g^{-1} during the first 20 cycles at a current density of 100 mA g^{-1}.[4] Up until now, it has still been a challenge to fully release the capacity of MnO_2.

Herein, we firstly report an almost complete and highly reversible conversion reaction of MnO_2 with a 4e process by utilizing 3D ordered hollow carbon spheres (HCS) as a conductive matrix. 3D ordered HCS are usually considered to be an excellent conductive framework due to their spherical shape, porosity and high specific surface area.[15,16] A PMMA emulsion was used as a template and resorcinol–formaldehyde as a carbon precursor to form HCS. The template was decomposed and then the precursor was carbonized into the uniform structure of HCS after sintering at 800 °C for 1 h under a N_2

State Key Laboratory of Physical Chemistry of Solid Surfaces, Department of Chemistry, College of Chemistry and Chemical Engineering, Xiamen University, Xiamen, Fujian, 361005, China. E-mail: qfdong@xmu.edu.cn; mszheng@xmu.edu.cn; Fax: +86-592-2185905; Tel: +86-592-2185905

† Electronic supplementary information (ESI) available: Detailed experimental procedures, XRD patterns, TGA, rate performance and discharge–charge curves. See DOI: 10.1039/c4ta00252k

‡ These two authors, Jun Zang and Jia Jia Chen, contributed equally to this work.

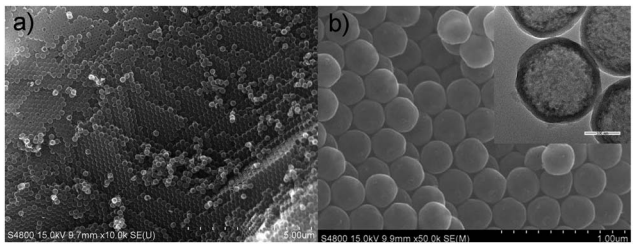

Fig. 1 SEM images (a and b) showing the morphology of 3D ordered HCS. The inset picture in (b) is a HRTEM image of the 3D ordered HCS.

atmosphere. As shown in Fig. 1a and b, all of the hollow carbon spheres form a close packed structure and are uniform in size with an average diameter of ~220 nm. A HRTEM micrograph (the inset picture of Fig. 1b) reveals that the carbon sphere shells have a uniform thickness of around 20 nm. The external surface of the HCS is very smooth and clean, indicating that no impurities were left over after the carbonization process. The HCS exhibit a type IV isotherm with a Brunauer–Emmett–Teller (BET) surface area of 922.56 $m^2\ g^{-1}$ and a mono-mesoporous size of around 4 nm, derived from N_2 porosimetry using the Barrett–Joyner–Halenda (BJH) method (see Fig. S1, ESI†).[17]

Nano-structured MnO_2 was grown *in situ* on the surface of HCS *via* a facile redox method, using P123 as a surfactant. $KMnO_4$ was reduced by the external carbon layer of HCS and then nano-crystalline MnO_2 was uniformly grown *in situ* on the 3D ordered surfaces of HCS, following the reaction process: $4\ MnO_4^- + 3C + H_2O \rightarrow 4\ MnO_2 + CO_3^{2-} + 2HCO_3^-$.[18] Composites with different MnO_2 ratios were obtained by adjusting the molar ratio of $KMnO_4$ and HCS, as determined by TG/DTA under a dry air atmosphere at a heating rate of 5° min^{-1}. The mass loading of MnO_2 was calculated to be 68%, 47% and 35% (see Fig. S2, ESI†). XRD patterns of the HCS and MnO_2/HCS composites with different MnO_2 loadings are shown in Fig. S3 (ESI).† The XRD peaks at $2\theta = 12°$, 37° and 66° can be readily indexed to the (001), (111) and (020) planes of birnessite-type MnO_2.[4] As the molar ratio of $KMnO_4$ increased, the extent of reduction of HCS gradually increased and the hierarchical structures of the MnO_2/HCS composites became severely damaged (Fig. 2a–d). For a low molar ratio of $KMnO_4$/HCS, MnO_2 could be uniformly grown on the surface of HCS. However, when $KMnO_4$ was in excess, the HCS in the composite almost disappeared (Fig. 2d). This indicates that only with a reasonable molar ratio of $KMnO_4$/HCS, can a uniform morphology and stable structure of MnO_2/HCS composite be obtained. As shown in Fig. 2b, the

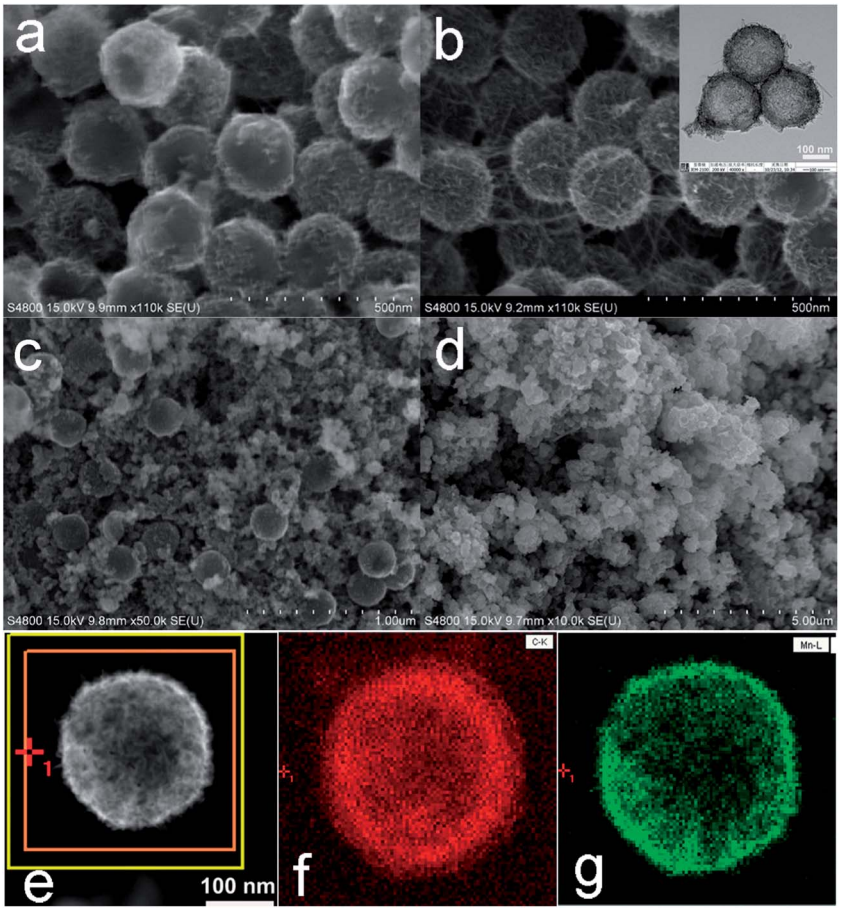

Fig. 2 SEM images showing the different morphologies of the MnO_2/HCS composites prepared by adjusting the molar ratio of $KMnO_4$/HCS: (a) MnO_2/HCS-35%; (b) MnO_2/HCS-47%; (c) MnO_2/HCS-68% and (d) pure MnO_2. The inset picture in (b) is a TEM image of MnO_2/HCS-47%. (e–g) A STEM image and the corresponding C and Mn elemental mappings of MnO_2/HCS-47%.

core–shell structure of the MnO_2/HCS-47% composite forms an interwoven 3D network structure with a size of ~100 nm in length and ~5 nm in width. The Mn and C element mappings (Fig. 2e–g) further confirm that the nano-structure MnO_2 has an intact interface with the surface of the HCS without significant fraction. The SAED pattern (see Fig. S4, ESI†) also clearly demonstrated that the as-prepared MnO_2 was nano-polycrystalline, which is in agreement with the results of the broadened XRD peaks of the MnO_2/HCS composites.

When tested as an anode material for lithium ion batteries, the electrochemical performance of the MnO_2/HCS composites were greatly influenced by their morphologies and hierarchical structures. As a conductive carbon matrix, HCS also exhibits superior rate and cyclic capability. No obvious fading of the discharge capacity was observed during 100 cycles after activation for the first 3 cycles under a current density of 0.1 A g^{-1} (Fig. 3a). In addition, it could maintain a stable capacity of 116.7 mA h g^{-1} at 10 A g^{-1} and had the ability to recover to almost 324.5 mA h g^{-1} when the current density returned to 0.1 A g^{-1} (see Fig. S5, ESI†).

Inspired by the stable electrochemical performance of HCS during the lithiation/delithiation process, nano-MnO_2 was grown *in situ* on the ordered HCS surfaces, with the aim of building novel composites with desirable electrochemical properties. As shown in Fig. 3a, most of the MnO_2/HCS composites experienced a marked fading in capacity during the initial cycles, which can be ascribed to lithium ion consumption during the decomposition of the electrolyte and the formation of a solid electrolyte interface (SEI) film. The MnO_2/HCS-47% composite exhibits the best electrochemical performance among all of the as-prepared products. It retains a stable capacity of 692.5 mA h g^{-1} (based on the whole mass of the MnO_2/HCS composite) during 100 cycles at 0.1 A g^{-1}, which is about 81% compared with the initial reversible capacity. MnO_2/HCS-35% shows stable cycling performance, but with a low specific capacity due to its low MnO_2 loading, while pure MnO_2 and MnO_2/HCS-68% deliver low capacities and suffer from capacity degradation during cycling, which are caused by the high active material mass loading and the destroyed structure of HCS.

Meanwhile, comparative studies of the voltage *versus* capacity profile at different rates (Fig. 3b) show that MnO_2/HCS-47% suffers a high rate discharge–charge testing with only small polarization. It presented typical electrochemical behavior, whilst delivering a reversible capacity of 420 mA h g^{-1} based on the whole mass of the composite at a current density of 1 A g^{-1}, which is still greater than the theoretical capacity of graphite (372 mA h g^{-1}). Even when increasing the current density up to 5 A g^{-1}, the composite could still deliver a specific capacity of 180 mA h g^{-1}. If the capacity contribution of HCS is subtracted from the MnO_2/HCS composite at the same current density (Fig. 3c, Fig. S5 and S6, ESI†), MnO_2 could achieve a stable reversible capacity of 1107.5 mA h g^{-1} at 0.1 A g^{-1} over 100 cycles, which is close to the theoretical value of 1233 mA h g^{-1}, indicating that an almost complete conversion reaction of MnO_2 was achieved during the lithiation/delithiation process. Nevertheless, the rate performance of the other MnO_2/HCS composites did not exhibit such stable or high capacity retention during cycling (see Table S1 and Fig. S7, ESI†).

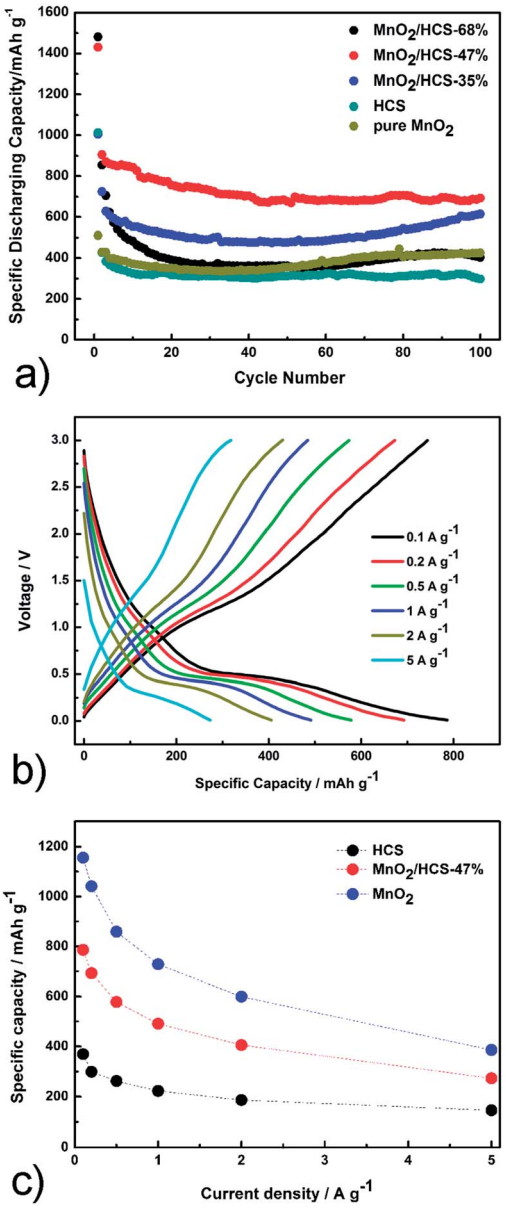

Fig. 3 (a) The cycle performance of the different mass loading MnO_2/HCS composites; (b) the charge–discharge curves of MnO_2/HCS-47% at different current densities; (c) the comparative rate performance of HCS, the MnO_2/HCS-47% composite and the capacity based on MnO_2 calculated by subtracting the capacity contribution of HCS from the MnO_2/HCS-47% composite.

If the electrochemical reaction between MnO_2 and Li can be described as a reversible 'conversion mechanism', then the formation of Mn/Li_2O should lead to a theoretical capacity of 1233 mA h g^{-1}. It is commonly believed that Li ion transport can be enhanced by the nano-structure, while electron mobility is highly dependent on the interface with the conductive matrix.[19] Therefore, the superior electrochemical performance of the MnO_2/HCS-47% composite can be attributed to the synergistic

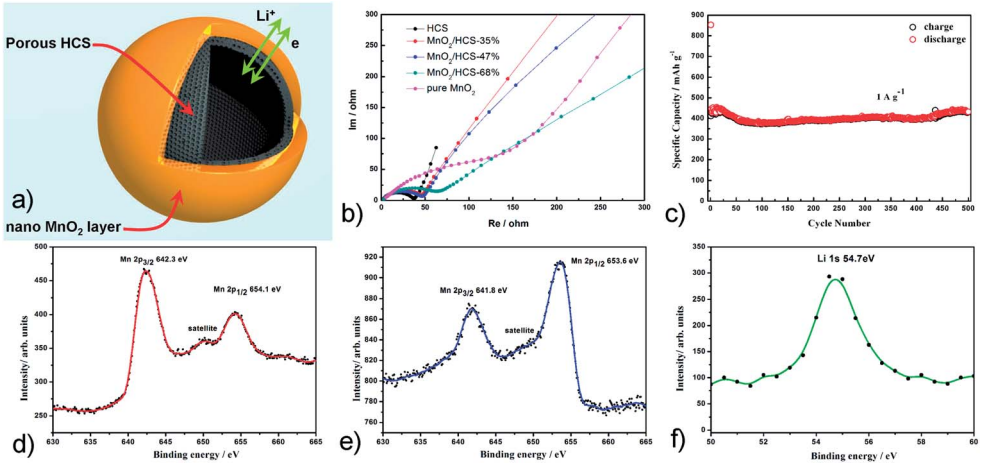

Fig. 4 (a) Illustration of the synergistic effect of hierarchical architecture of core–shell MnO_2/HCS composite; (b) comparative AC impedance studies of HCS, pure MnO_2 and different MnO_2 mass loading MnO_2/HCS composites; (c) long cycling and high rate testing of MnO_2/HCS-47% at 1 A g^{-1}, specific capacities were calculated based on the whole mass of MnO_2/HCS-47% composite; and XPS spectra of Mn element in MnO_2/HCS-47% composite before (d) and after (e) first discharge process. Formation of Li_2O (f) during the initial lithiation process has been confirmed using XPS.

effect of the hierarchical architecture. As illustrated in Fig. 4a, the high porosity of HCS facilitates the penetration of electrolyte into the nanopores, while the high specific surface area is favorable for increasing electron transfer within the spherical structure. Meanwhile, HCS shows excellent structure stability during the Li^+ intercalation/deintercalation process, even when subjected to a very high current density. After the *in situ* growth of MnO_2 on the ordered surfaces of HCS, Li^+ diffusion and electron transfer at the interface of the nanoscale MnO_2 and HCS can be greatly improved. As confirmed by EIS (Fig. 4b), HCS has the lowest charge transfer resistance (R_{ct}), while the R_{ct} of the MnO_2/HCS composites increases as the mass loading of MnO_2 increases. Meanwhile, in the XPS results showing the Mn 2p spectrum (Fig. 4d), the peaks for Mn $2p_{3/2}$ and $2p_{1/2}$, which are centered at 642.3 and 654.1 eV, respectively, with a spin–energy separation of 11.8 eV, are in good agreement with previously reported data.[3,20] At the end of the first discharge of MnO_2/HCS-47%, an XPS peak of Li 1s centered at 54.7 eV appears, confirming the formation of Li_2O. And the binding energies of Mn $2p_{3/2}$ and $2p_{1/2}$ decrease due to the reduction of MnO_2 to metallic Mn (Fig. 4e and f).[3,21] According to the results of XPS spectrum, MnO_2 can be reduced into Mn and Li_2O in the initial lithiation process. Considering the highly reversible charge–discharge capacity of 1107.5 mA h g^{-1}, an almost complete conversion reaction of MnO_2 can be achieved in MnO_2/HCS-47%. The advantage of the synergistic effect of the hierarchical architecture can be further confirmed by studying the exceptionally long cycle performance under a high current density (Fig. 4c). There is no obvious capacity fading over 500 cycles and the composite retains a stable 420 mA h g^{-1} specific reversible capacity when tested at 1 A g^{-1}. This excellent electrochemical reversibility and structural stability could be ascribed to the unique hierarchical structure, which can withstanding the huge volume changes during the charge–discharge process.

Conclusions

In summary, we have prepared a MnO_2/HCS composite with a hierarchical hollow structure. A thin layer of poorly crystallized birnessite-type MnO_2 can be homogeneously grown *in situ* on the external surface of HCS. The superior electrochemical performance can be attributed to the synergistic effect of the hierarchical architecture. Firstly, the conductive HCS matrix improves the ion and electron transportation in the MnO_2 bulk phase, while also decreasing the resistance at the interface of the electrode/electrolyte. Secondly, the intact interface of nano-MnO_2 with the surface of HCS provides good elasticity retention, retarding the volume changes during Li^+ insertion/extraction in the MnO_2 bulk phase and thus facilitating repetitive cycling. Last, but not least, such a unique structure of a hollow core–shell MnO_2/carbon composite will probably have potential applications in electrochemical power sources, sensors and other fields, such as catalysts for lithium–air batteries.

Acknowledgements

We gratefully acknowledge financial support from the Key Project of NSFC (U1305246, 21321062), and the Major Project funded by Xiamen city (3502Z20121002).

Notes and references

1 P. Poizot, S. Laruelle, S. Grugeon, L. Dupont and J.-M. Tarascon, *Nature*, 2000, **407**, 496.
2 P. L. Taberna, S. Mitra, P. Poizot, P. Simon and J. M. Tarascon, *Nat. Mater.*, 2006, **5**, 567.
3 V. B. R. Boppana and F. Jiao, *Chem. Commun.*, 2011, **47**, 8973.
4 F. Y. Cheng, J. Chen, X. L. Gou and P. W. Shen, *Adv. Mater.*, 2005, **17**, 2753.

5 S. Chen, J. Zhu, X. Wu, Q. Han and X. Wang, *ACS Nano*, 2010, **4**, 2822.
6 M. Kundu, C. C. A. Ng, D. Y. Petrovykh and L. Liu, *Chem. Commun.*, 2013, **49**, 8459.
7 A. L. M. Reddy, M. M. Shaijumon, S. R. Gowda and P. M. Ajayan, *Nano Lett.*, 2009, **9**, 1002.
8 C. X. Guo, M. Wang, T. Chen, X. W. Lou and C. M. Li, *Adv. Energy Mater.*, 2011, **1**, 736.
9 Y. Wang, Z. J. Han, S. F. Yu, R. R. Song, H. H. Song, K. (Ken) Ostrikov and H. Y. Yang, *Carbon*, 2013, **64**, 230.
10 J. Zhao, Z. Tao, J. Liang and J. Chen, *Cryst. Growth Des.*, 2008, **8**, 2799.
11 M. S. Wu and P. C. Chiang, *J. Phys. Chem. B*, 2005, **109**, 23279.
12 M. V. Reddy, T. Yu, C. H. Sow, Z. X. Shen, C. T. Lim, G. V. Subba Rao and B. V. R. Chowdari, *Adv. Funct. Mater.*, 2007, **17**, 2792.
13 L. Shen, H. Li, E. Uchaker, X. Zhang and G. Cao, *Nano Lett.*, 2012, **12**, 5673.
14 L. Li, A.-R. O. Raji and J. M. Tour, *Adv. Mater.*, 2013, **25**, 6298.
15 Y. Li, T. Li, M. Yao and S. Liu, *J. Mater. Chem.*, 2012, **22**, 10911.
16 F. Böttger-Hiller, P. Kempe, G. Cox, A. Panchenko, N. Janssen, A. Petzold, T. Thurn-Albrecht, L. Borchardt, M. Rose, S. Kaskel, C. Georgi, H. Lang and S. Spange, *Angew. Chem., Int. Ed.*, 2013, **52**, 6088.
17 A. Lu, A. Kiefer, W. Schmidt and F. Schüth, *Chem. Mater.*, 2004, **16**, 100.
18 Z. Lei, J. Zhang and X. S. Zhao, *J. Mater. Chem.*, 2011, **22**, 153.
19 D. Wang, D. Choi, J. Li, Z. Yang, Z. Nie, R. Kou, D. Hu, C. Wang, L. V. Saraf, J. Zhang, I. A. Aksay and J. Liu, *ACS Nano*, 2009, **3**, 907.
20 D. Liu, Q. Zhang, P. Xiao, B. B. Garcia, Q. Guo, R. Champion and G. Cao, *Chem. Mater.*, 2008, **20**, 1376.
21 M. C. Biesinger, B. P. Payne, A. P. Grosvenor, L. W. M. Lau, A. R. Gerson and R. S. C. Smart, *Appl. Surf. Sci.*, 2011, **257**, 2717.